

A Nondestructive Method of Grain Microstructure Determination

Joyce Lai

Department of Energy-Office of Science, Science Undergraduate Laboratory Internship (SULI)

University of California at Berkeley

Stanford Linear Accelerator Center

Stanford, California

August 14, 2004

Prepared in partial fulfillment of the requirements of the Office of Science, Department of Energy's Science Undergraduate Laboratory Internship under the direction of Apurva Mehta in the Stanford Synchrotron Radiation Lab Division at Stanford Linear Accelerator Center.

Participant:

Signature

Research Advisor:

Signature

Table of Contents

Abstract	iii.
Introduction	1
Procedure	2
Results and Discussion	5
Conclusions	8
Figures	10
Table	15
References	16
Acknowledgments	17

Abstract

Locating the Sources of a Diffraction Pattern Via a Triangulation Algorithm for Ray-Tracing.

JOYCE LAI (University of California at Berkeley, Berkeley, CA, 94720) APURVA MEHTA

(Stanford Linear Accelerator Center, Stanford, CA).

Customarily, a material has been sectioned to study its internal grain microstructure and thus in the process is destroyed. Using x-rays, however, there are two nondestructive methods of determining the sources of diffraction spots and hence the internal grain microstructure of a sample. One technique consists of placing a wire in the path of a diffracted ray so that its image is prevented from appearing on the detector screen. Ray-tracing is then done to locate the source within the sample from whence the rays emanate. In this experiment, we investigate the other technique of determining source location by recording diffraction patterns at ten equally-spaced detector distances and then graphing the data with reasonable-fit lines using the least-squares fitting routine. We then perform a ray-tracing triangulation technique to pinpoint the location of the source from which the rays are coming. Cluster analyses are employed and plots of ray number versus pixel position of certain points at some particular detector distances are created. An error propagation analysis is then carried out as a check to the cluster analyses and graphs of error deviation along the detector path versus ray number are constructed. With statistical error analyses and construction of error boxes using chosen pixel error deviations and delta z error values, the best error measurement using the detector method was found to be plus/minus 100 microns. In this study, it was found that the detector method provided a much poorer resolution than the traditional wire technique of which there is a source size precision of within 1-5 microns. The detector method, though, is sufficient for large-grain material studies.

Introduction

Traditionally, to study its internal grain microstructure, a sample must be sectioned and thus destroyed. The application of x-rays, however, enables us to look at the internal structures of materials without destroying the samples because they penetrate through the material and are diffracted by grains to produce intricate but analyzable diffraction patterns [5]. By knowing the positions of two sets or more of at least two collinear points, a triangle can be traced out through triangulation whose vertex is the location of the source.

When an x-ray beam from a synchrotron ring is directed toward a sample, the beam penetrates through the material and may be diffracted by a single grain or crystal to produce a diffraction pattern on a detector. For a multigrain sample, the diffraction pattern contains spots from rays that originate from more than one source or grain within the sample and if the rays can be traced back to their origins, one can locate the grains buried inside the sample without sectioning the material. Two types of triangulation to determine the source(s) of diffraction spots are currently used. One uses a moving wire and a fixed detector. The other involves changing the distance of the detector from the sample.

In the wire technique, a wire approximately one centimeter in length and a few microns in diameter is scanned over the sample. When the moving wire blocks a certain ray from appearing as a spot on a detector, it locates its position [1]. Therefore, by knowing the position on the wire where the ray was blocked and the position of the missing spot on the detector, the ray can be traced back to its origin inside the sample.

In the study at hand, the other technique to determine the source(s) of diffraction spots is tested. This method involves collecting diffraction patterns for ten different detector distances. Triangles are formed through linear regression whose sides are the ray lines. This triangulation algorithm was applied to the diffraction pattern data for sapphire recorded at the Advanced Light

Source of the Lawrence Berkeley National Laboratory by Apurva Mehta and Monica Barney.

Determination of the number of sources, thus, will enable us to know the crystal orientations in the material and also the locations of those grains within the sample. Error analyses are performed to determine the precision and robustness of the source locations.

The wire method is more precise than the method we are using in this experiment because the wire can be placed very close to the sample so that the error involved in the estimation of direction of the ray can be made very small. In carrying out the other technique, the complication arises in that the detector cannot be moved too close to the sample due to physical constraints such as certain apparatuses attached to and surrounding the detector that protrude or jut out which would strike the sample if the detector was moved too close. Through the employment of these two different methods of source determination and comparing the extent of error in each technique, we will be able to see whether the detector method gives us precision comparable to the wire method.

Procedure

The diffraction patterns originated from 2-mm thick parallelepiped sapphire (aluminum oxide) rods that were annealed to either side of a rectangular piece of aluminum through ultra-high vacuum diffusion bonding [2]. The sample was mounted on a motorized x-y-z stage angled at 45 degrees to a 0.8 x 0.8 micron 5-14 KeV beam of x-rays. The sample was moved horizontally during the experiment so that the synchrotron beam “traveled” from sapphire to aluminum and back to sapphire. As aluminum is very soft and its diffraction patterns are distorted, ray-tracing was first performed on the diffraction data for sapphire. From this, it was hoped that the microstructure of sapphire could be characterized and in turn, the same procedure might be carried out to analyze the aluminum diffraction patterns. Data for fifty positions at

every two microns across the sample was recorded, but the analysis of only three positions, 8, 10, and 12, is presented.

During the experiment, the beam was directed at a specific location on the sample where it penetrated the material and was diffracted by the grains in the sample, giving rise to a diffraction pattern on a detector equipped with a charge-coupling device. After this pattern was recorded, the detector was moved back ten millimeters. This process was repeated for eight more detector distances, for example from 395 to 385 to 375 mm. The most number of spots appeared on the pattern detected at the nearest detector position (see Figure 4) and likewise, the fewest number at the farthest detector position (see Figure 3). Each time the detector moved back, it intercepted a smaller solid angle of rays and therefore recorded fewer and fewer spots. Hence, one bright spot on the detector at the farthest position could be traced back through where it appeared on each of the other patterns at their respective detector distances to locate the source. Of these thirty-four peaks, twenty-two were chosen and tracked because these were the brightest spots and hence the most easily seen.

The x-coordinate values of each of twenty-two marked diffraction spots at one detector distance of a position were determined through a peak search using version 4.0 of the X-Ray Microdiffraction Analysis Software developed by Nobumichi Tamura of the Advanced Light Source of Lawrence Berkeley Labs. It was then seen that only thirty-four peak intensities (discernable bright spots) appeared on every pattern detected at each detector position. The x-coordinate values for these peaks were recorded and tabulated on Excel spreadsheets. Certain curve distributions that fit the x-coordinate values such as the centroid fit type, the 2D Gaussian, 2D Lorentzian, and 2D Pearson were examined for any disparities from one another of which there were none up to 0.001 pixels. The points were graphed with detector distance as the abscissa and the x-coordinate values (as pixel position) in the ordinate (see Figure 1). Best-fit

lines were then accommodated to the data using the least squares curve-fitting routine of linear regression. From this, the slope and intercept of each of the twenty-two best-fit lines were obtained. By using the method of least-squares [3], both the standard deviations of the slope and intercept of each best-fit line could also be determined through the LINEST function of Excel. The standard deviation values were checked to see whether the lines were reasonable fits. Following this, the ray lines were extrapolated (see Figure 2) so that a convergence point could be seen and the graph axes were formatted to focus on the point of convergence. It was surmised that the lines would converge to a single point—the source of the rays. However, the rays did not intersect at exactly one point (see Figure 5).

To attempt to resolve this issue, cluster analyses were first performed. These were accomplished by noting which line series made up each cluster in the position. Each line series would pertain to the same spot that was followed through the ten detector distances and a cluster would be the vertex of the triangle that was constructed using linear best-fit lines through x-coordinate points as its sides. The lines were followed from left to right of the graph so that it could be seen which cluster a particular line intersected first.

For example, if a ray intersected Cluster B first (see Figure 5), it would not be counted in any other cluster it intersected later on because it would already have reached and indicated the location of the source grain that diffracted it. For Position 10, it was recorded which rays or line series constituted each of clusters A, B, and C and hence which diffraction spots came from each source, since each cluster most likely represented a source crystal. Then combinations of two clusters were analyzed by seeing which lines remained that were not part of either cluster. In total then, three combinations of two clusters were examined from three choices of clusters.

Afterwards, error analyses were done by plotting ray number versus pixel position (see Figure 6). This was achieved through drawing a vertical line through the rays whose endpoint

intersected with the x-axis. It could then be seen what rays intersected the vertical line at specific pixel positions at that position of the x-axis. Using these graphs, the pixel error could be determined by examining the flat regions of the lines. We could then say which ray lines constituted a cluster and so made up a single source. We could also determine the number of possible sources in that particular sample from whence the rays were coming and their positions in the sample.

An error propagation analysis [4] was then done as a check to the previous cluster analyses to observe the standard deviation of each of the best-fit lines. The error propagation relation $\Delta z = z * \sqrt{(\Delta b/b)^2 + (\Delta m/m)^2}$, where Δm and Δb refer to the error in the slope and intercept of each line respectively, was used to determine Δz , the error uncertainty along the axis of detector movement. A ray number versus delta z graph was then created. To keep track, the marked spots under study were noted on a separate diagram. This was repeated for the diffraction patterns at the other detector distances for sample Position 10 and also for Positions 8 and 12 to determine whether the delta z error values were comparable to each other.

Results and Discussion

For purposes of brevity, only selected results are displayed. Because the standard deviations of the slopes and intercepts were less than one percent, they indicated reasonably-fit lines. For Position 10, the cluster analysis suggested that there were at least two clusters in that position, and hence, at least two well-defined sources. There are the fewest remaining rays that do not intersect with either Cluster B or C when considering rays that intersect with only these two intersections. Therefore, it can be certain that there is a source at each of clusters B and C (see Figure 5). The same procedure performed for Positions 8 and 12 reveal the same result—that the same Clusters B and C each made up a possible source.

The source from whence the rays making up Cluster B originate is about 0.1 mm, or 100 microns, and is about 441.174 mm from the origin (see Figure 5), set past the farthest detector distance. Thus, if the distance between the closest detector distance and the sample is known, regardless of the angle the sample is oriented relative to the beam, a precise location for the source can be pinpointed within the sample given that the source is 441.174 mm from the origin and that the sample is at most 2 mm in thickness. For this case, to know the location of a grain that is diffracting the rays, we need only subtract the distance of the origin from the spot where the horizontal beam penetrates the sample from 441.174 mm. We can then know how far within the sample, along the axis the beam is traveling, the source is. Likewise, the rays that compose Cluster C are from a source that is also about 100 microns but is about 441.297 mm from the origin. This would point to a different crystal or grain within the sample at beam Position 10 that the rays are emanating from.

It is further verified that certain rays are from one source and the other rays are from the other source in the creation of plots of ray number versus pixel for Position 10 (see Figure 6). The rays are ordered from the bottom to the top and the points 441.174 mm and 441.297 mm were used because by eyeing the midpoints of the intersections, it appeared that the midpoints of the clusters were situated at those points. When the data is arranged so that pixel position corresponds to the ordinate axis and the ray number to the abscissa axis, flat regions on the graph can be observed. These flat regions mean that for successively increasing ray numbers from the bottom to the top at point 441.174 mm, for example, the pixel position value does not change considerably and hence, the rays that fall within the flat region would be the rays that compose the source. The slanted regions of the graph, then, would represent the spacing differentiation between certain clusters of rays and would be used to distinguish among intersections.

The pixel error deviation can be measured by noting the change in range of the pixel position values from the beginning to the end of the flat region plateau (see Figure 8). From Figure 8, we can determine the pixel error to be about 0.005 pixels. Based on this pixel ordinate value, an error box with pixel error deviation as its height can be constructed around the rays which will determine how many rays make up that source and the size of the source. The lengths of the box would be constructed by drawing and extending lines horizontally until the lines touched rays. This intersection of box length and ray would make up a corner of the error box. Thus, an estimate of the error in the 'z' position (along the axis that the detector is moving) of each source can be reached. The size of the source can also be known by noting the length of this box. Using this method of error determination, an error of plus or minus 0.005 pixels was obtained for Cluster B at point 441.174 mm of Position 10 and, accordingly, the size of the source pointed out by Cluster B was approximately 100 microns, as was found by the earlier error propagation study.

The ray number versus delta z graph (see Table 1 and Figure 9) indicates that whereas some of the error is as low as 0.1 mm, or 100 microns, there is also error up to plus/minus 10 mm, or 10,000 microns! If we consider the deviation to be 100 microns though, we can determine how many sources there are in this case. For example, taking only the horizontal into consideration, given an error of plus/minus 100 microns, any line intersecting in Cluster B cannot deviate more than to the endpoints of the blue box width limit (see Figure 10) and the same for Cluster C. Hence, we arrive at two relatively well-defined sources. Suppose, now, that we consider an error of plus/minus 200 microns. Then the rays have a probability of intersecting anywhere within the pink box size width limit and the farthest points of deviation now extend horizontally so that there would be an overlap of intersection of lines. Upon examination of the graph then, no distinct sources would be discerned and the entire graph would appear to be a

conglomeration. An error of only 100 microns, on the other hand, could well define the number of sources in this case. The 100-micron error, then, is consistent with the results from the cluster analysis. However, because some rays are poorly defined, the estimation of two possible sources is not reliable.

The points 441.174 mm and 441.297 mm were selected by visual examination of the cluster graphs. As a result, the plots of ray number versus pixel position may contain some bias. Hence, for an unbiased cluster location, several equally-spaced cluster graphs could be created (such as for every 10 microns along 'z', the axis of detector movement). Then the plot showing the graph with the flattest slope will indicate the tightest cluster there and will correspond to the location of the source.

Conclusions

In this research, it was seen that x-rays could be used to look at the depth profile of a material without sectioning or destroying it. Also, ray-tracing could be performed through diffraction pattern spots and based on this, we could see that the location of the sources depended on how well the rays were traced back.

The detector technique of profiling the depth of the source in the sample gave a best source size of within plus or minus 100 microns, whereas the statistical analysis results from the wire method as conducted by Gene Ice et al. at Oak Ridge National reported a source size within 1-5 microns [6]. The former method, then, is at least twenty times less precise than the latter. Even the best rays have 100 micron uncertainty, which is large compared to the 5 micron uncertainty of the wire technique. Hence, further investigations are needed on why some errors of Δz were large as compared to other values. Unfortunately then, we do not yet know the number of sources because there is no explanation yet for why some rays are more well-defined than others. Thus, if an experiment requires high resolution, the wire technique is needed. But

for experiments that do not need high resolution or precision, such as of large-grain aluminum in the data of Barney and Mehta, the detector method is sufficient. In future studies, perhaps greater precision in the former method can be attained using more detector distances spread over a large region. Some change to the experimental setup must be implemented to allow even closer detector placement.

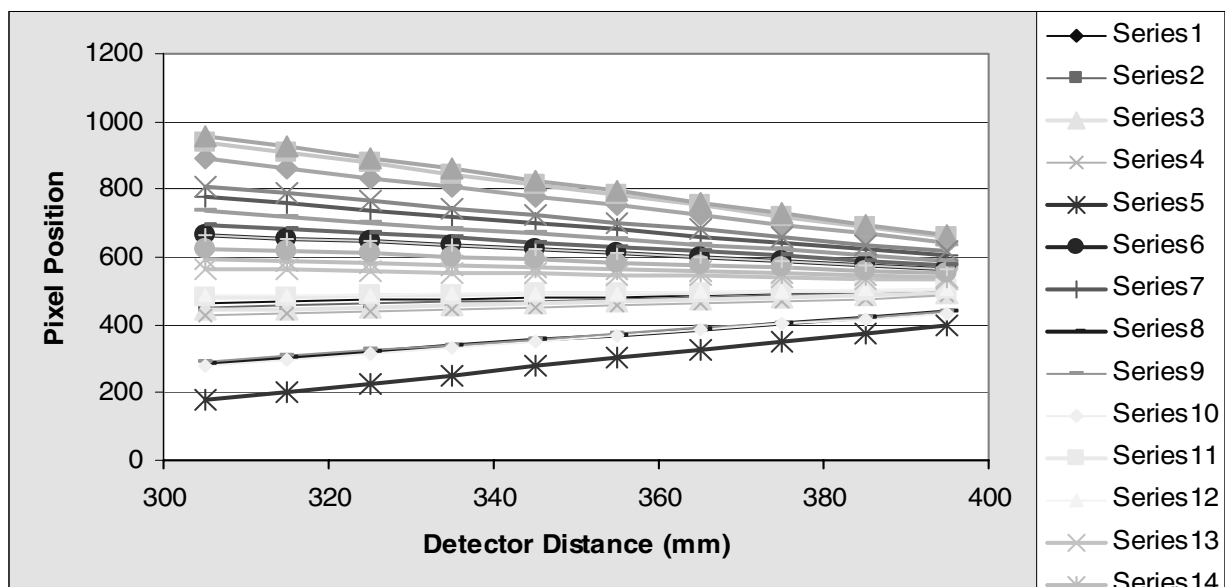


Figure 1. X-coordinate values of diffraction spots to detector distance fitted by lines using the least squares method. Each of the lines designated by different colors represents one spot that is traced through the ten detector distances to reconstruct the path of a ray.

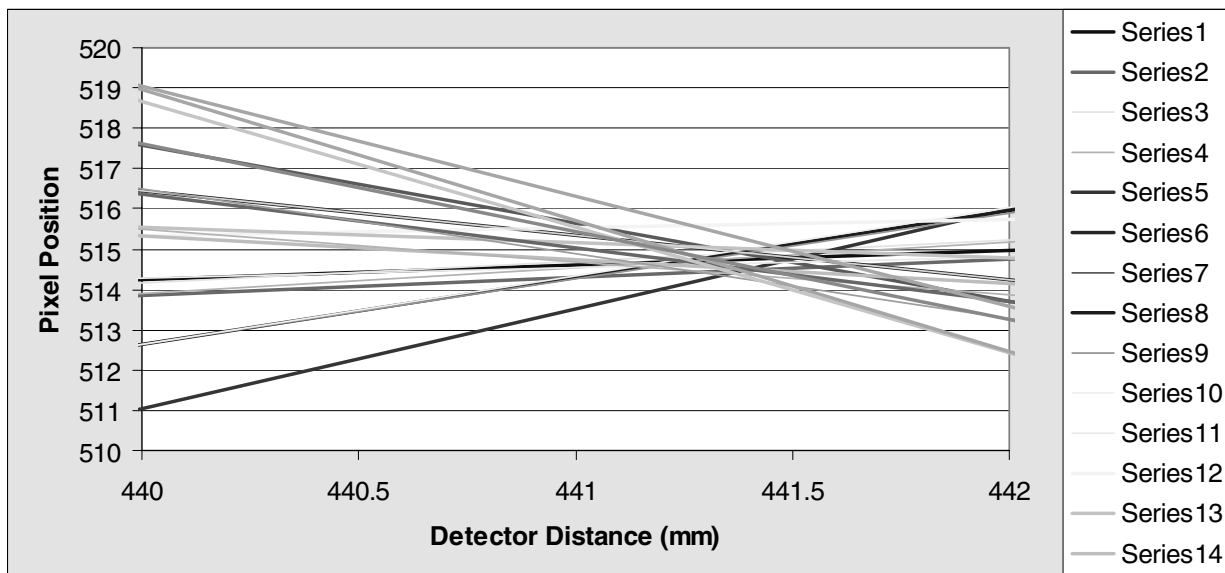


Figure 2. Extrapolation of ray lines to see a general convergence point.

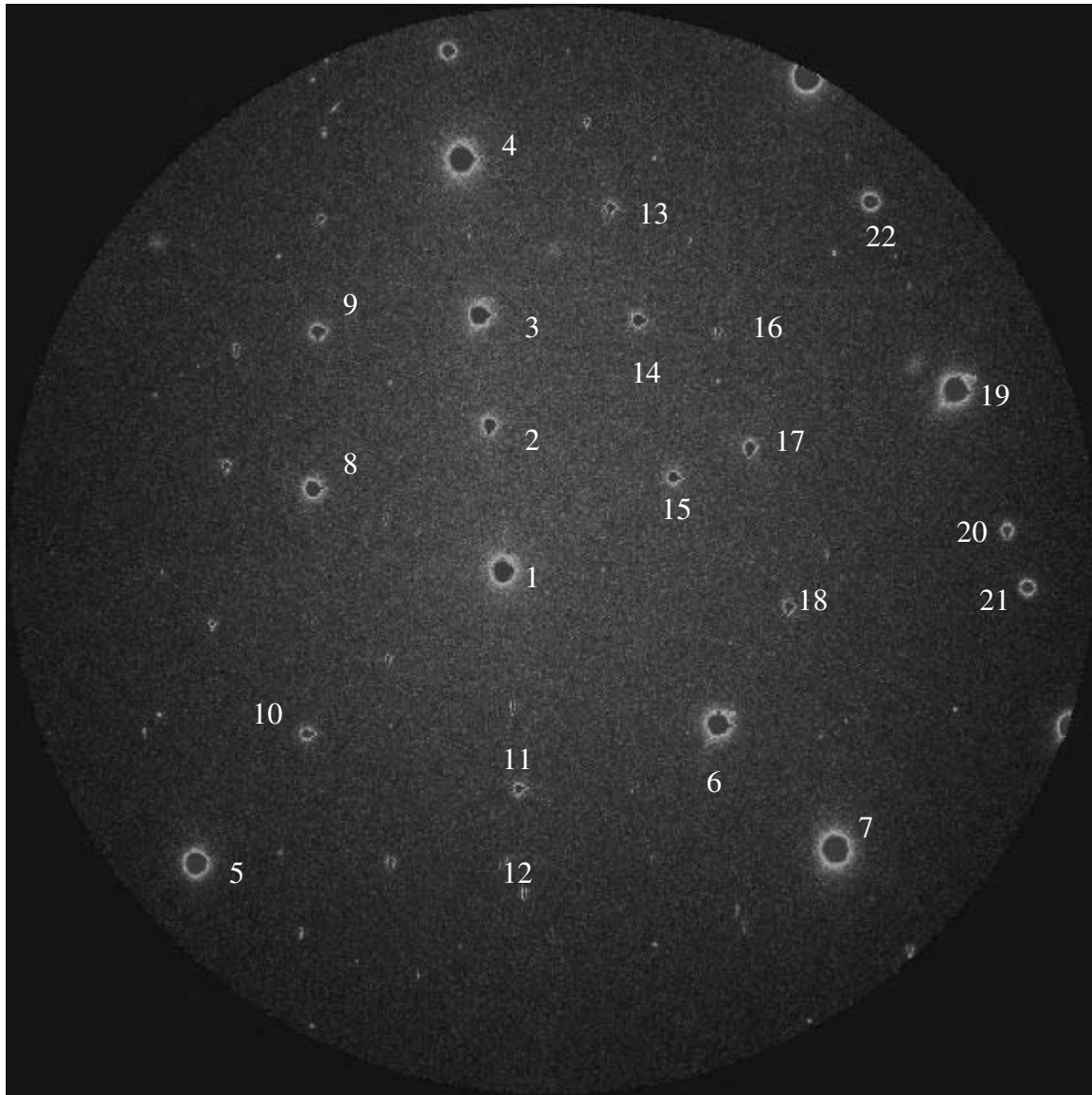


Figure 3. Sapphire diffraction pattern at farthest detector position of 305 mm of sample position 10 showing the twenty-two bright spots studied.

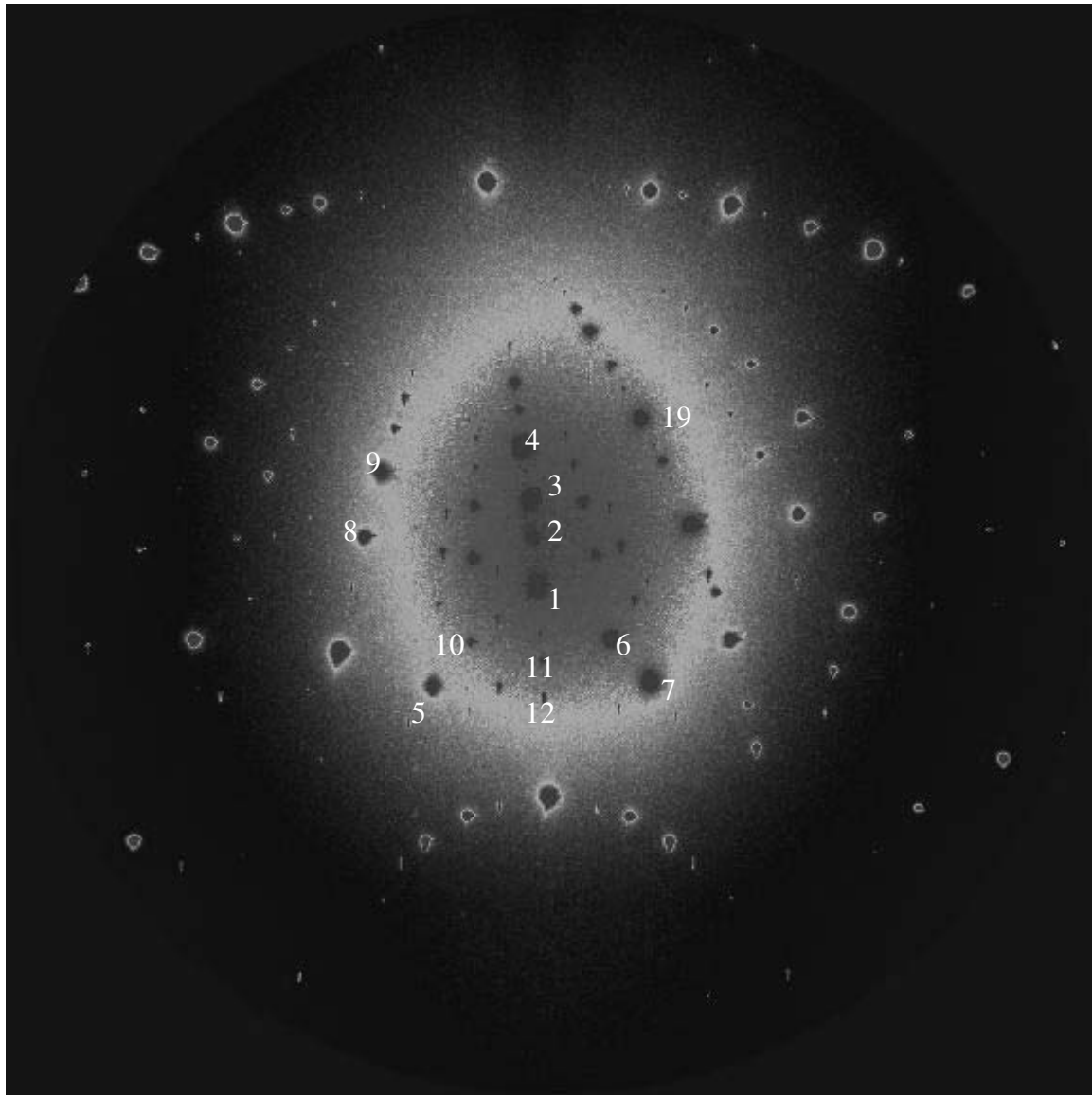


Figure 4. Sapphire diffraction pattern at nearest detector position of 395 mm of sample position 10 showing bright spots.

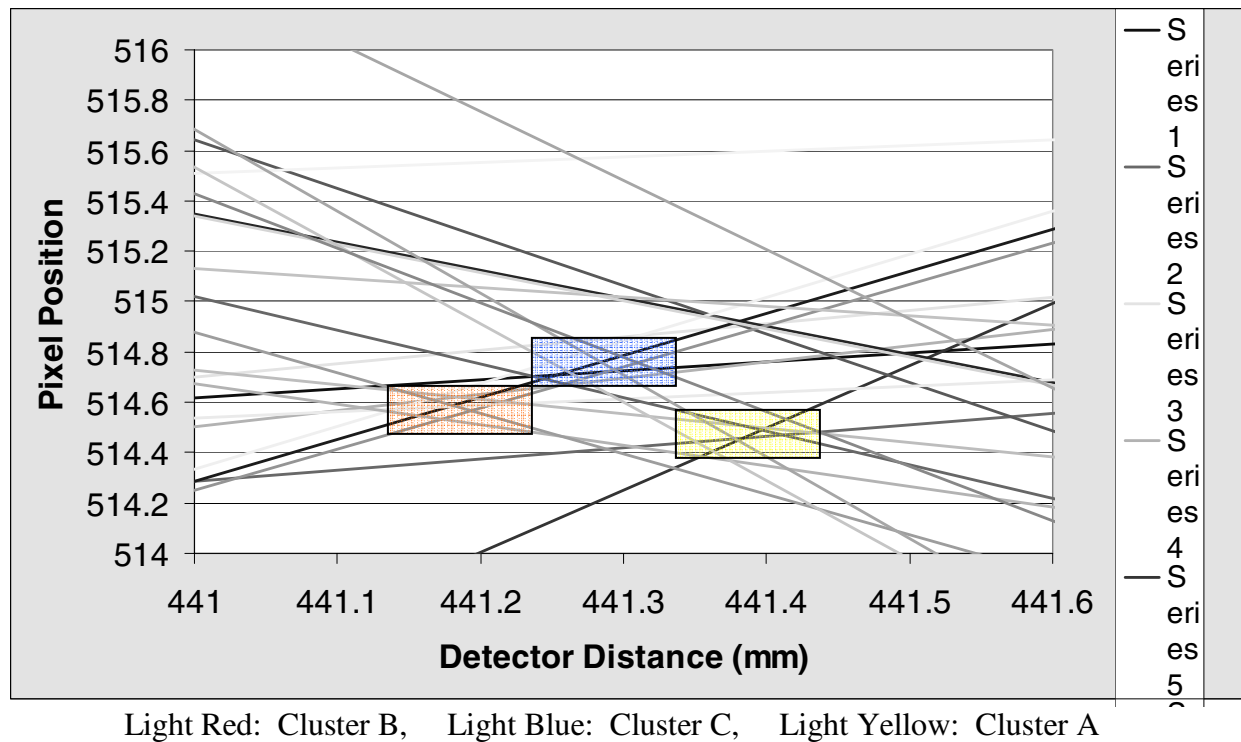


Figure 5. Focusing on the point of convergence of the ray lines. Lines do not intersect at exactly one point. There are as many as three major intersections which could each denote a source from whence rays are coming.

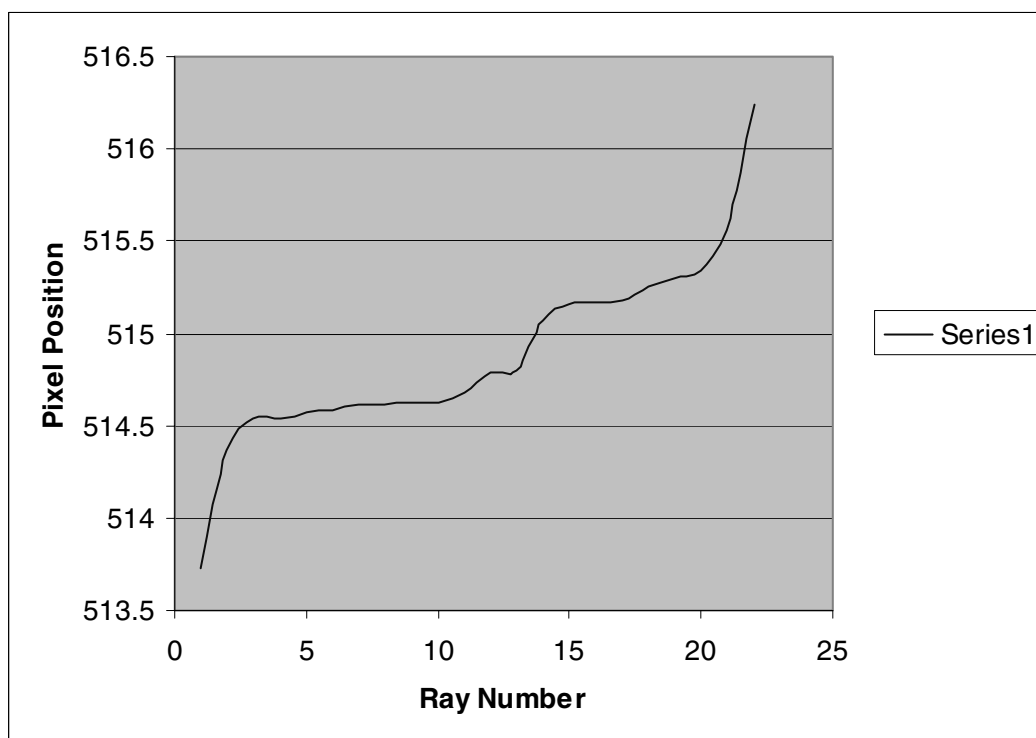


Figure 6. Pixel position to ray number for Cluster B at detector distance 441.174 mm. The pixel error deviation can be measured by noting the change in range of pixel values from beginning to end of flat region plateau. The pixel error deviation is used to construct error boxes.

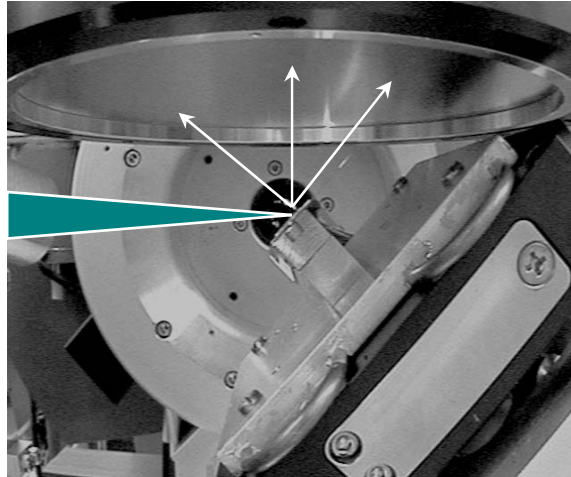


Figure 7. Experimental setup. X-ray beam (green triangular shape) is directed toward sample of material mounted on a ledge and is diffracted, producing a diffraction pattern on the detector.

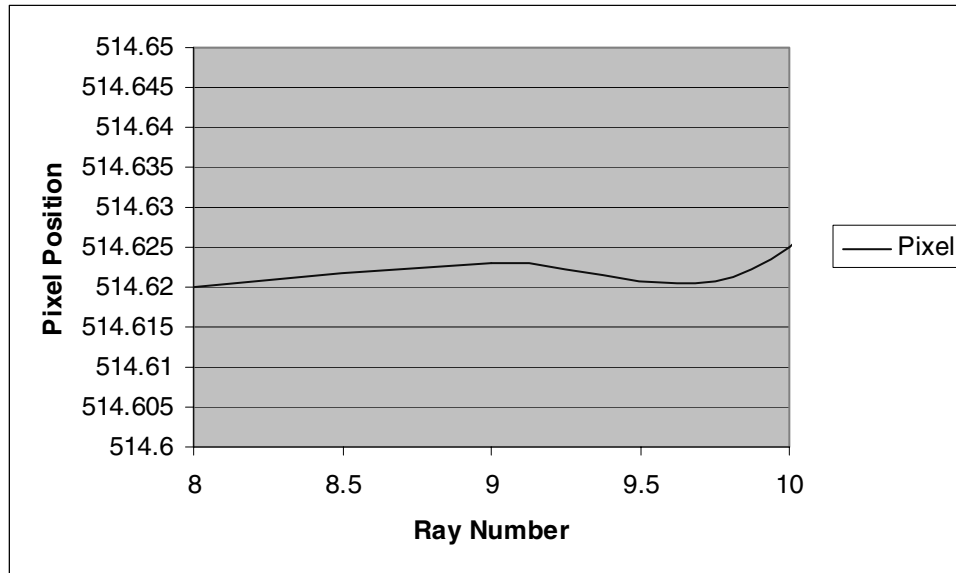


Figure 8. Zoom-in of first flat region of Figure 6. An error of plus/minus 0.005 pixels was obtained for Cluster B at this point 441.174 mm of Position 10.

Series	Δz	Series	Δz
1	0.11226	12	0.891571
2	0.119077	13	0.920582
3	0.161702	14	1.297021
4	0.266186	15	1.346842
5	0.356338	16	1.469097
6	0.36748	17	1.608911
7	0.410865	18	1.623347
8	0.461597	19	2.023984
9	0.558075	20	2.206733
10	0.722624	21	2.84745
11	0.865897	22	9.965727

Table 1. Delta z error values for each of the twenty-two lines as calculated from the error propagation relation.

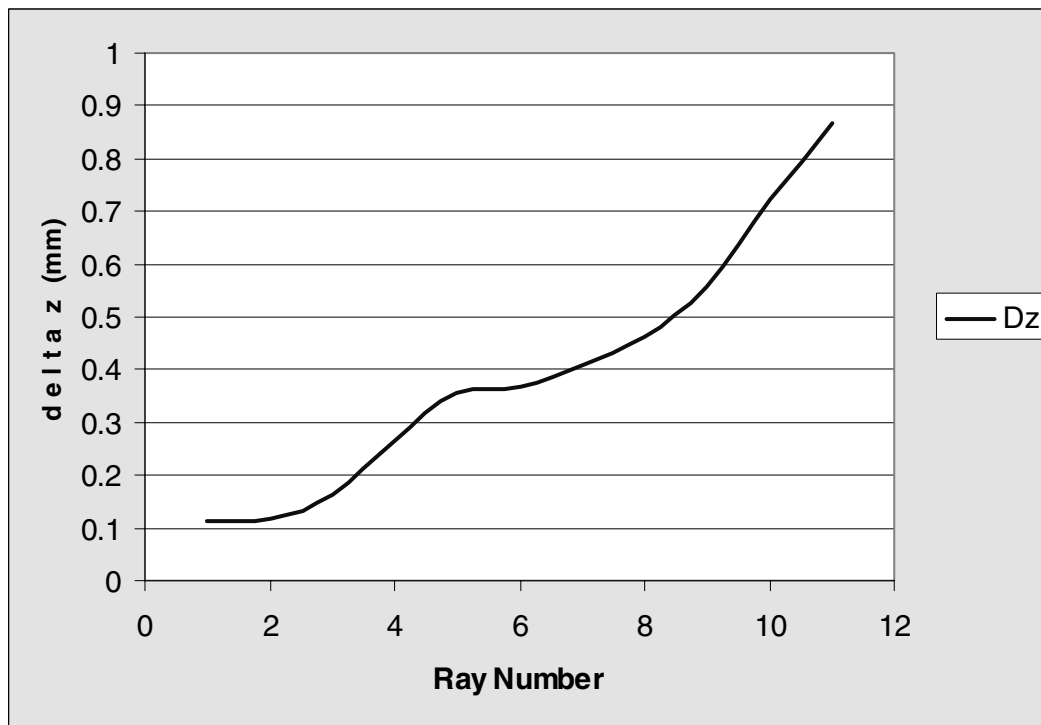


Figure 9. Graph of Table 1. Whereas some of the error, delta z, is as low as 0.1 mm, or 100 microns, there are also delta z error values up to plus/minus 10 mm, or 10,000 microns.

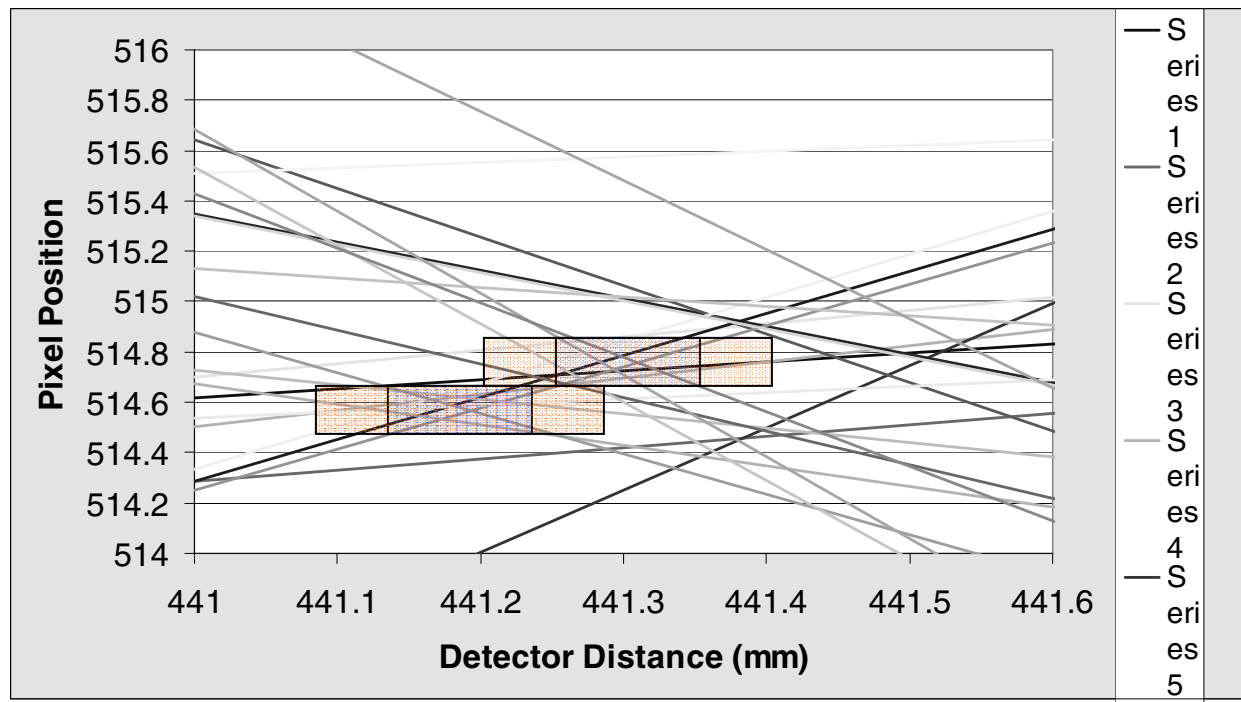


Figure 10. Error boxes of 100 micron width (blue boxes) and 200 micron width (red boxes) constructed for Clusters B and C.

References

- [1] B.C. Larson, B. Lengeler, "High-Resolution Three-Dimensional X-Ray Microscopy," *Materials Research Society Bulletin*, vol. 29, No. 3, Mar. 2004, pp. 152-156.
- [2] Callister Jr., W.D., *Materials Science and Engineering: An Introduction*, John Wiley and Sons, Inc., New York, 2003.
- [3] Beers, Y., *Introduction to the Theory of Error*, Addison-Wesley Publishing Company, Inc., Massachusetts, 1962.
- [4] Clifford, A.A., *Multivariate Error Analysis: A Handbook of Error Propagation and Calculation in Many-Parameter Systems*, Applied Science Publishers LTD, London, 1973.
- [5] Cullity, B.D., S.R. Stock, *Elements of X-Ray Diffraction*, Prentice Hall, New Jersey, 2001.
- [6] W. Hardin, "X-Ray System Gives 'In-Depth' Look at Crystal Properties," *The International Society for Optical Engineering-OE Magazine*, Dec. 2002, p. 8.

Acknowledgments

I would like to thank Apurva Mehta, from whom my fascination for my project was derived, for providing such good guidance and for telling me not to turn back in the midst of adversity and abandon what I had already made progress on. He enabled me to see light in a dark room and for that, I will be forever grateful. Thanks to Samuel Webb for assistance in the data analysis and Monica Barney for allowing me to examine her data. I also thank the Department of Energy and the Stanford Linear Accelerator Center for letting me take part in such a wonderful and exciting program dedicated to creating the next generation of scientists who may be the key to unlocking the many mysteries of the world.